Experimental study of the chemical vapor deposition from CH3SiHCl2/H2: Application to the synthesis of monolithic SiC tubes

P. Drieux, G. Chollon, S. Jacques, A. Allemand, D. Cavagnat, T. Buffeteau

Experimental study of the chemical vapor deposition from CH_3SiHCl_2/H_2: Application to the synthesis of monolithic SiC tubes

P. Drieux[*1,2], G. Chollon[1], S. Jacques[1], A. Allemand[1,2], D. Cavagnat[3], T. Buffeteau[3]

[1]*LCTS, Université Bordeaux 1 - CNRS UMR 5801*

Allée de la Boétie, 33600 Pessac, France

[2]*CEA Le Ripault, 37260 Monts, France*

[3]*ISM, Université Bordeaux 1 - CNRS UMR 5255*

Cours de la Libération, 33405 Talence, France

**Corresponding author: drieux@lcts.u-bordeaux1.fr*

(0033)556844726

Abstract

The aim of the present work is to synthesize high strength monolithic SiC tubes to improve the imperviousness of a SiC/SiC composite structure. A few hundred micrometers-thick tubular coatings were produced by chemical vapor deposition (CVD) at atmospheric pressure, from $CH_3SiHCl_2/Ar/H_2$ mixtures. The CVD-SiC tubes were obtained by deposition on the inner walls of a SiO_2-tube substrate, previously coated with a pyrocarbon interfacial layer to promote delamination. A continuous deposition process was developed to allow the realization of relatively long CVD-SiC tubes, by sliding the heating system along the substrate. The chemical composition and the microstructure of the tubes were studied by electron probe microanalysis, Raman spectroscopy and scanning electron microscopy.

The deposition rate, composition and microstructure of the CVD-SiC coatings were investigated as a function of the substrate temperature and the gas flow rates. A Fourier transformed infrared (FTIR) spectroscopy analysis was carried out at the reactor outlet to characterize the gas phase reactions. The FTIR analysis of pure species from the Si-C-Cl-H system as well *ab initio* calculations at the density functional theory (DFT) level allowed the assignment of the main IR features in the experimental spectra and the

quantitative analysis of the complex gas mixture. This study has led to the proposal of a simplified dichloromethylsilane decomposition scheme which is consistent with the influence of the CVD parameters on the nature of the gas phase and the coating. The deposition rate, the Si/C atomic ratio, the SiC crystalline state and the surface morphology are indeed strongly related to the CH_3SiCl_3 decomposition rate and the further progress of homogeneous reactions.

Keywords

CVD, atmospheric pressure, Silicon carbide, nuclear fuel cladding, gas phase analysis

1. Introduction

Generation IV nuclear energy systems are next-generation technologies that will allow a more efficient use of the nuclear fuel and provide a better operating safety. They are expected to be available around 2040. Tubular SiC/SiC composites [1, 2] are materials of prime interest to be part of the nuclear fuel claddings of future power plants [3-6], thanks to their low neutron activation characteristics [7] but also their high strength and fracture toughness at high temperature [8].

The optimization of SiC/SiC composites for nuclear purposes requires high thermal properties as well as excellent gas imperviousness [9]. The latter point has implied the need of an additional sealing layer. Lately, several concepts have appeared with the will to place this layer around a single SiC/SiC composite layer [10], or between two composite layers, as a liner [11]. A few refractory metallic materials, such as Tantalum, have shown a good compatibility with the composite structure, but a SiC_{β} sheath, having high specific mechanical properties, no porosity, as well as an excellent stability at high temperature and under neutron irradiation, might as well ensure this function.

SiC monofilaments are exemplary CVD-SiC materials in terms of mechanical properties [12]. They are prepared by chemical vapor deposition at atmospheric pressure (APCVD) on a hot filament substrate, using chlorosilanes (e.g. dichloromethylsilane: DCMS) diluted in hydrogen as the SiC precursor [13, 14]. A failure strength up to 6 GPa and an ultimate strain of about 1.5 % can indeed be reached by the high performance SCS-Ultra commercialized by Specialty Materials Inc. On the basis of the CVD-SiC filament processing experience, the aim of the present study is to prepare SiC tubes by APCVD, with a composition, microstructure and morphology compatible with high strength and strain at failure.

In this study, the synthesis of monolithic SiC tubes by APCVD from the DCMS/H_2 system and the characterization of their properties are detailed. A particular attention is given to the chemical composition, the structure of the coatings and their growth rates, all of them depending on the deposition parameters. Fourier transform infrared (FTIR) analyses of the gas phase at the reactor outlet have been performed to follow the decomposition of the precursor during the process and the IR spectra were confronted to *ab initio*

calculations at the density functional theory (DFT) level of the theoretical features of the different chlorosilanes likely present in the gas phase. The correlation between all these experimental approaches has led to the proposal of a simplified gas phase reaction and deposition mechanism.

2. Experimental

The APCVD reactor presented in Figure 1 consists of a horizontal silica glass tube (L = 1000 mm, $\emptyset_{int}$ = 46 mm) connected to gas inlet/outlet flanges at both ends. Dichloromethylsilane (CH_3SiHCl_2, DCMS, 97%, from Sigma Aldrich) was used as the SiC precursor rather than other precursors (such as CH_3SiCl_3, MTS, which is more often industrially used), because of its low decomposition temperature [15] and its high vapor pressure (P_{DCMS} = 48 kPa at 20 °C) favoring a use at atmospheric pressure. These properties led the choice of the DCMS/H_2 system for the synthesis of CVD-SiC monofilaments [13]. The DCMS vapor saturation was obtained from a H_2 carrier gas going through a bubbler maintained at 20°C. The DCMS concentration was adjusted by further diluting the initial saturated DCMS/H_2 mixture in a secondary H_2 flow.

The inside of a silica tube (L = 500 mm, $\emptyset_{int}$ = 8 mm) was used as a substrate. A thin layer of pyrolytic carbon (PyC) was deposited at the surface of the SiO_2 tube in order to prevent chemical bonding between the substrate and the coating. The PyC interfacial layer was deposited in the same reactor by sliding the heating bench and by injection of pure propene at low pressure (Q_{C3H6} = 100 sccm, T = 1000°C, P = 3 kPa). The tube was brought to high temperature by a surrounding graphite susceptor heated by induction. This unit was placed inside the large silica glass tube and connected to the inlet flange in order to force the gas mixture to flow inside the substrate tube. The process was in a hot-wall configuration, since the whole 8 mm diameter reaction chamber, including the substrate walls, was isothermal in the hot deposition area (4 cm). The surface temperature (T) of the graphite shell outer surface was monitored *in situ* during the CVD process with a high-resolution dichromatic pyrometer (Impac ISQ 5).

In order to manufacture relatively long silicon carbide tubes, the induction heat station was set on a motorized bench allowing the induction coil −andthus , the hot area− to slide along the silica tube and the substrate. The sliding speed of the heating bench, named hereafter *S*, can range from 0.25 to 5 cm/min.

For this study, the temperature T and total gas flow Q_{tot} ranged from 1100 to 1200°C and from 250 to 1000 sccm (standard $cm^3.min^{-1}$), respectively. This parameter range is slightly modified compared to our previous work [16].

The morphology of the coatings was characterized with a field emission gun scanning electron microscope (SEM) (FEI Quanta 400F).

Electron probe microanalyses (EPMA) (SX 100 from CAMECA, France) were conducted on cross-sections of the CVD-coated SiO_2 substrate parallel and perpendicular to the tube axis. The Si, C and O concentrations were assessed using the wavelength dispersive spectroscopy (WDS) mode (10 kV, 10 nA). Pure SiC and SiO_2 were use as standards. The carbon content was deduced by difference to avoid errors due to surface contamination. The error in the concentrations is approximately 1 at. %. Punctual and line scan measurements were performed along the cross section of the coatings, with a lateral resolution of approximately 1 μm^2.

Raman microprobe (RM) analyses (Labram HR from Horiba Jobin Yvon) were also conducted on the same specimens. The excitation source was a He–Ne laser (λ=632.8 nm). The power was kept below 1 mW to avoid heating of the sample. The lateral resolution of the laser probe was close to 1 μm and the depth analyzed was less than 1 μm. As for EPMA, punctual and line scan analyses were recorded along the cross section of the deposit.

A quantitative study of the gas phase was carried out by Fourier transform spectroscopy (FTIR) at the reactor outlet. The IR beam of the spectrometer (Nicolet 550) was led through a room temperature analysis cell (with two ZnSe windows at both ends, L = 50 cm) installed at the reactor outlet (absorption configuration). While the reaction chamber was set at atmospheric pressure, the pressure in the gas cell was adjusted to 1 kPa to avoid saturation of the absorption peaks on the FTIR spectra. At the outlet of the gas

cell, the infrared beam was focused on the HgCdTe MCT-A detector placed below. The whole infrared beam path was enclosed and constantly purged with a nitrogen flow in order to limit the absorption of atmospheric compounds. A background spectrum was first recorded with a pure H_2 flow in the reactor and subtracted to the reacting gases spectrum. The apparatus allowed the acquisition of spectra in the wavenumber range 600 - 4000 cm^{-1}, with a resolution of 1 cm^{-1}.

3. Theoretical calculations of IR spectra

The geometry optimizations, vibrational frequencies and absorption intensities were calculated by Gaussian 09 program [17] on the DELL cluster of the MCIA computing center of the University Bordeaux I. Calculations of the optimized geometry of CH_3SiHCl_2 (DCMS), CH_3SiCl_3 (MTS), SiH_3Cl, SiH_2Cl_2, $SiHCl_3$ (TCS) and $SiCl_4$ were performed at the density functional theory level using B3LYP functional [18, 19] and cc-pVTZ basis set. Vibrational frequencies and IR intensities were calculated at the same level of theory. For comparison to experiment, the calculated intensities were converted to Lorentzian bands with a half-width of 4 cm^{-1}. To obtain a detailed assignment of each compound, the potential energy distribution (PED) for each mode has been determined, in the harmonic approximation, according to the method developed by Allouche [20].

4. Results

4.1.Synthesis of monolithic tubes : influence of the experimental conditions

Following the continuous PyC deposition described in the experimental section, the silicon carbide synthesis was realized in both continuous and static conditions. The PyC interlayer exhibits a thickness of 350 nm which does not introduce major surface flaws at the substrate/SiC coating, and partly stays adherent to the coating after cooling, hence requiring a further removal by oxidation (Figure 2). A list of representative experiments conducted in static configuration is given in Table I.

Both EPMA and SEM measurements around the perimeter of cut rings confirmed the chemical composition and thickness homogeneity of the coatings. The oxygen concentration was found to remain lower than 2 at.% in all specimens.

Deposition runs in static configuration have been mainly conducted in order to study the influence of the deposition parameters on the growth rate and the stoichiometry of the coating.

Whatever the single source precursor [14, 16-21] used (CH_3SiCl_3, $(CH_3)_2SiCl_2$, CH_3SiHCl_2), the key parameters in the deposition of SiC by CVD are the temperature, the total pressure, the global gas flow rate (or residence time) and the nature of the precursor dilution, characterized by the α ratio:

$$\alpha = Q_{H_2} / Q_{DCMS}$$

The Si/C atomic ratio increases significantly with α (Table I). At a temperature of 1100 °C and for a total flow rate of 500 sccm, when α increases from 0 to 12, the silicon atomic concentration in the coating varies from 45 at.% to 68 at.%, *i.e.* from a carbon excess to a very significant silicon excess. An important dilution of DCMS in H_2 also results in a strong decrease of the deposition rate. It should be mentioned that in comparison to our previous work [16], growth rates have been greatly improved by the forced injection of the gas mixture inside the substrate. Hence, even high dilutions of the precursor result in deposition rates above 100 µm/h. For moderate α values, *i.e.* for $1 < \alpha < 4$, a maximum of 930 µm/h can be achieved, which is high enough to synthesize both long and thick tubes in a relatively short period of time. After reaching this maximum, the deposition rate decreases at particularly low α values, as already observed for the CH_3SiCl_3/H_2 system [21]. Together with the increase of deposition rate, it is worthy of note that solid particles tend to grow from the gas phase beyond 1100°C and for low α values. These solid products seem to appear and deposit at the tube outlet, in cool parts, as already observed for $DCMS/C_3H_8/H_2$ [14] or $(CH_3)_2SiCl_2/H_2$ systems [22]. This phenomenon could be due to the polymerization of light instable species [23] and is probably favored by high pressure and low precursor dilution.

The Raman spectra (Figure 3) show clear Raman features assigned to crystalline SiC (expected at 750-1000 cm^{-1}) in the deposits [24] at low α values, but also a strong peak around 520 cm^{-1}, typical of free

silicon. The intensity of the Si band varies with α in very good agreement with the excess silicon expected in the coating, as deduced from the EPMA measurements.

A gradual improvement of the SiC crystalline state can be noticed when the deposition temperature increases. For $\alpha = 4$, $Q_{tot} = 500$ sccm and when the deposition temperature increases from 1100 °C to 1200 °C, the emergence of two sharp characteristic bands in the 750 – 1000 cm^{-1} region of the Raman spectra confirms the increasing amount as well as the coarsening of the SiC phase. In parallel, the narrow peak at 520 cm^{-1} as well as the 500 cm^{-1} bump due to crystalline and amorphous Si, respectively, both disappear, indicating lower excess silicon at high temperature. The Si/C atomic ratios obtained by EPMA are very consistent with the Raman analyses. Only a few changes in the deposition rate can be noticed with the variation of temperature, with a mean value as high as nearly 1 mm/h.

The influence of the total gas flow rate was examined in a next step. When Q_{tot} increases from 250 sccm to 1000 sccm (T = 1100 °C, $\alpha = 4$), the silicon concentration, as measured by EPMA, tends to increase from 51 at.% to 65 at.% (see Table 1). These results are consistent with the Raman analyses (Figure 3) showing that the peak assigned to crystalline Si tends to disappear at low Q_{tot} while simultaneously, the SiC characteristic bands gradually appear. The deposition rate increases significantly with Q_{tot} from 440 µm/h at 250 sccm, to a maximum of 1170 µm/h at 1000 sccm.

For all these studies carried out in static conditions, the chemical compositions and deposition rates correspond to the maximal thickness of the coating, located in the hot part of the deposition area. At both sides of this hot zone, the drop of the induction power (*i.e.* of the temperature) leads to major modifications of both chemical composition and thickness. These changes have to be properly characterized, since the whole temperature profile will affect the deposition conditions at a given position of the substrate during the continuous process. Figure 4 shows the evolution of chemical composition along the coating, which is typically 4.5 cm long in static runs. A decrease of the carbon content can be noticed when temperature drops at both ends of the tube. This phenomenon is more significant at the outlet side of the tube, indicating that temperature is not the only parameter causing these changes.

Using a continuous process, samples of a thickness up to 200 µm were successfully synthesized by sliding the induction coil at low velocities (S ranging from 0.25 to 0.5 cm/min). Tubes as long as 25 cm were obtained, demonstrating the feasibility of the process. The chemical composition of the coating is consistent with the results obtained in static conditions. Homogeneous tubes along the axis having a Si/C ratio of 1 in the radial central zone were indeed produced at high temperature (T = 1200 °C), medium flow rates (Q_{tot} = 500 sccm) and low dilutions (α = 2 to 4). The radial composition profile (along the thickness) of a particularly thick tube elaborated in heat stage sliding conditions (S = 0.25 cm/min) (T = 1200 °C, Q_{tot} = 1000 sccm, α = 2), has been compared to the axial profile (along the gas flow direction) of a tube synthesized in the same CVD conditions but in static configuration. The total thickness (e) and the radial composition profile through the thickness of the tube wall ($C_{Si}(\varepsilon)$) obtained in sliding conditions, are indeed directly related to the longitudinal deposition rate and concentration profiles obtained in static configuration (respectively $R(x)$ and $C_{Si}(x)$), since $d\varepsilon = 1/S\, R(x)dx$.

Both Raman and EPMA analyses exhibit a similar evolution of the chemical and phase compositions. The presence of free silicon was indeed observed in the part of the coating corresponding to the beginning of the deposition during the continuous process (Fig. 5), *i.e.* to the low temperature and low maturation conditions in the static configuration, at the entrance of the heated zone (Fig. 4).

4.2.Gas phase analysis

The changes in the chemical composition of the deposit are related to the variations of the temperature on the concentration of the effective silicon and carbon precursors brought to the deposition area. FTIR analyses of the gas phase at the reactor outlet were performed so as to determine how the modification of the gas phase with temperature affects the deposition process. This study will allow linking the gas phase composition changes with the structural and chemical properties of the coating.

In a first step, the infrared spectra of DCMS and species potentially encountered in the gas mixture (such as $SiHCl_3$ (TCS) and $SiCl_4$) were recorded at room temperature (Figure 6). The main bands observed

in the IR spectra as well as those reported in the literature [25-30] are given in the Table II. The assignment of these bands has been performed from the *ab initio* at the B3LYP/cc-pVTZ level and PED calculations performed during this study. The calculated frequencies and intensities of the vibrational modes as well as their assignment on the basis of the normal modes are reported in the supporting information (Table i to Table vi) for DCMS, MTS and chlorosilanes (SiH_3Cl, SiH_2Cl_2, $SiHCl_3$ and $SiCl_4$). It is noteworthy that the frequencies of the stretching vibration of the CH_3 and SiH_n groups are overestimated due to anharmonic effects (scaling factors of 0.96 and 0.98 can be used for the stretching vibration of the CH_3 and SiH_n groups, respectively).

The infrared spectrum of DCMS shows the presence of a weak band at 2984 cm^{-1} corresponding to the antisymmetric stretching vibration of the methyl groups (ν_aCH_3), a very sharp and intense band at 2217 cm^{-1}, due to the stretching vibration of Si-H bond, a low intensity signal at 1268 cm^{-1} corresponding to symmetric bending vibration of the methyl groups (δ_sCH_3) and a conglomerate of intense peaks in the 900 – 650 cm^{-1} region, due to the bending vibrations of HCSi and HSiCl (889 and 852 cm^{-1}) and to the stretching vibration of Si-C bond. The IR bands exhibits PQR or PR profiles characterizing the coupling of vibrations with rotation. The infrared spectra of $SiCl_4$ and TCS compounds are easier to interpret. IR spectrum of $SiCl_4$ reveals only one band at 620 cm^{-1}, assigned to the antisymmetric stretching vibration of $SiCl_4$ (ν_aSiCl_4). Finally, the IR spectrum of $SiHCl_3$ (TCS) compound exhibits three main bands at 2260 cm^{-1} corresponding to the stretching vibration of Si-H bond, at 807 cm^{-1}, corresponding to the bending vibration of HSiCl and at 590 cm^{-1}, due to the antisymmetric stretching vibration of $SiCl_3$ (ν_aSiCl_3).

An investigation of the temperature effect on the gas phase composition was carried out in a second step. The infrared spectra recorded at room temperature after heating the gas phase at various temperatures, ranging from 25 to 1250 °C, are reported in Figure 7. Whereas the spectra remains unchanged from 25 °C to 700 °C, major chemical modifications appear at higher temperatures. As the analysis is carried out *ex situ* at room temperature, the detected molecules are necessarily stable and some of them may result from the recombination of unstable intermediates (e.g. free radicals). Furthermore, at high temperature, where the

deposition rate becomes significant, some part of them might be consumed through heterogeneous reactions leading to the SiC deposition. Hence, the consumption of DCMS, the apparition of new species at the reactor outlet and their possible consumption due to homogeneous or heterogeneous reactions provide useful information for a better understanding of the APCVD process. The decomposition of dichloromethylsilane in the reactor is accompanied by the formation of HCl, $SiHCl_3$, SiH_2Cl_2, $SiCl_4$ and CH_4 (Fig. 7). The formation of unsaturated hydrocarbons such as C_2H_2 was also observed, but only at very high temperatures.

To follow the evolution of the gas phase with the raising temperature, the temperature dependence of several IR bands associated with the DCMS precursor or with the new produced species was investigated. One or two bands were selected per species, after verifying that these bands did not overlap with other neighboring IR bands. Thus, the bands at 2217 and 756 cm^{-1} have been chosen for DCMS, 2260 and 807 cm^{-1} for $SiHCl_3$, 950 cm^{-1} for SiH_2Cl_2 and 620 cm^{-1} for $SiCl_4$. For the CH_4 species, the PQR profile in the 3220-2820 cm^{-1} spectral range as well as the only Q band of the antisymmetric stretching vibration ($\nu_a CH_4$) at 3017 cm^{-1} have been considered, subtracting the HCl contribution for each temperature. For the HCl species, three bands at 2843, 2821 and 2798 cm^{-1} have been considered. In this study, the analysis was pushed a step further by converting the qualitative monitoring (area of the bands *vs* temperature) into quantitative data (concentration of species *vs* temperature). For this purpose, available pure products (DCMS, $SiHCl_3$, $SiCl_4$, CH_4 and HCl) were analyzed in the FTIR cell at various pressures (*i.e.* at various concentrations, considering the perfect gas equation C=P/RT) in order to determine the molar absorptivity for each band following the Beer-Lambert law:

$$\int A(\nu) = \int \varepsilon(\nu) \cdot L \cdot C \qquad (1)$$

where $\int A(\nu)$ is the integrated absorbance for a band, $\int \varepsilon(\nu)$ the molar absorptivity for the considered band, L the length of the analysis cell (0.5 m) and C the concentration of the gas phase. The molar absorptivity $\int \varepsilon(\nu)$ (in $cm.mol^{-1}$) can be directly related to the calculated intensity of the band, $I(\nu)$ (in $km.mol^{-1}$) by the relationship:

$$I(\nu) = 0.023 \int \varepsilon(\nu) \quad (2)$$

The evolutions of the concentration with temperature are reported in supporting information (Figure i and Figure ii) for several bands of $SiHCl_3$ and other pure products derived from DCMS. The values of $I(\nu)$ determined from these figures are in good agreement with those determined by *ab initio* calculations (table i and table v in supporting information). A good agreement has also been obtained for the antisymmetric stretching vibration of $SiCl_4$ at 620 cm^{-1} (I=537.4 $km.mol^{-1}$ from experimental data *vs* I=542.4 from *ab initio* calculations). As some mismatch between experimental and calculated values was observed for CH_4 and HCl species, only the theoretical values were considered. The infrared spectra recorded from pure species indeed did not allow the assessment of a consistent $\int \varepsilon(\nu)$ coefficient, probably due to peak overlapping or on insufficient spectral resolution.

Using the molar absorptivity determined experimentally for DCMS, $SiHCl_3$ and $SiCl_4$ and calculated for SiH_2Cl_2, CH_4 and HCl, in the Beer-Lambert relation (1), it was then possible to plot the evolution of concentration of the different species versus the temperature, as shown in Figure 8. For the DCMS and TCS compounds the results were averaged from the bands at 2217 and 756 cm^{-1} and at 2260 and 807 cm^{-1}, respectively (see supporting information Figure iii and Figure iv). Figure 8 reveals a progressive formation of CH_4 and HCl during heating, starting beyond 700 °C, while DCMS is simultaneously consumed. This modification of the gas phase is essentially due to kinetic effects (the DCMS decomposition rate being activated by the temperature rise). Even at high temperature, when DCMS is fully decomposed, only a part of the species expected at thermodynamic equilibrium [31] is observed experimentally by FTIR spectroscopy. This is mainly due to the *ex situ* conditions, which imply that only stable products can be evidenced at room temperature. A thermo-kinetic modeling of the DCMS/H_2 system (e.g. on the basis of the work of Ge and Gordon [32]) is in progress to accurately describe these changes of gas phase. The evolution of the respective Si and Cl containing compounds seems to be related. A gradual chlorination of the chlorosilane species can be noticed : SiH_2Cl_2 first appearing from 750 °C and then reaching a maximum at 850 °C, followed by $SiHCl_3$, reaching a maximum at 950 °C and finally $SiCl_4$, substituting for the two

others at high temperatures as the major silicon bearing species found at the reactor outlet. The global decrease of the various products starting at 1200 °C might correspond to heterogeneous reactions, *i.e.* to the formation of the coating or other solid byproducts appearing in larger amounts at this temperature. The decrease of the HCl concentration is surprising however; as it is rather expected to keep on increasing with T [31]. This could be related to the reaction of chlorine species (such as HCl) with the Si-rich regions from the surface at high temperature, as suggested by the decrease of both deposition rate and silicon content of the coating [31, 33]. The formation of the solid condensates at the outlet of the tube might as well have led to gas depletion or a pressure drop downstream. This would explain the decrease of the deposition rate as well as the general concentration decrease observed for all species at 1100 and 1200°C (including HCl, chlorosilanes and CH_4).

5. Discussion

The deposition of SiC on the inner walls of the SiO_2 tube and the use of a pyrocarbon interphase is a very promising method for obtaining smoothed net-shape SiC tubes. The anisotropy of PyC promotes the SiC/SiO_2 interface delamination. The silicon carbide tube can easily be extracted from the silica substrate by taking advantage of the perfectly flat SiO_2/SiC interface and the thermal expansion coefficients mismatch between the silica and the SiC.

The investigation of the influence of the various experimental deposition parameters on the coating gives information about the type of regime controlling the CVD process in the explored conditions. For $T \geq 1100$ °C, the deposition process is apparently not thermally activated, rather suggesting a mass transfer-limited regime [35]. This is confirmed by a strong dependence of the deposition rate on the gas flow rate, as also reported in previous studies [33, 36]. However, since the temperature increase results in parallel in important changes of the composition of the gas phase (and therefore of the local concentration of the effective Si and C precursors) in the hot area, the usual assumption of a precursor supply limitation should be considered with care. The increase of the deposition rate with Q_{tot} and with the optimization of injection

conditions [16] is also indicative of a regime limited by diffusion. The gas velocity is an important parameter especially in the case of a mass transfer regime where the deposit morphology can be very sensitive to the gas flow around the substrate. In addition, Q_{tot} may affect the decomposition rate of precursors through the residence time, which varies along the position in the hot area. The change in the composition of the deposit suggests a major effect of the maturation of gas phase, *i.e.* of the decomposition rate of DCMS into various intermediates, which may act as effective precursors of Si and C for the coating.

A sufficiently high deposition temperature is required to form a near stoichiometric and highly crystalline coating. Whereas there are only a few studies on the CVD from DCMS/H_2 [13-14, 37-38], several articles on the dichlorodimethylsilane (DCDMS)/H_2 system [37, 39-40] and an abundant work on the MTS/H_2 system [12, 21, 31-34] can be found in the literature. Féron *et al.* used the DCMS/H_2 system ($\alpha = 2,3$) at atmospheric pressure in a cold wall reactor to synthesize monofilaments ($\emptyset = 200$ µm) [14]. They always obtained Si-rich coatings (Si/C at. > 1.4) with much higher deposition rates (4000 µm/h at 1200 °C), according to a chemical reaction controlled regime, for T < 1200 °C. This confirms the occurrence of a strong DCMS depletion in the present case, in a hot wall configuration and with a much higher S/V ratio. On the other hand, Cagliostro *et al.* used $(CH_3)_2SiCl_2$ (DCDMS) at similar temperatures and pressure in a hot wall reactor configuration [39, 40]. They found a dependence of the deposition rate with the total flow rate for T > 900 °C and a strong silicon excess in the coating, decreasing along the reactor axis (*i.e.* while the residence time increases). A similar behavior was reported in several studies of the MTS/H_2 system in relatively similar T and P conditions. Papasouliotis *et al.* and Huttinger *et al.* indeed evidenced, for T = 1000 °C, a decrease of both the deposition rate and the silicon excess along the hot zone [21, 41-42]. The decreasing of the total flow rate also leads to a drop of the deposition rate (due to increase of the residence time) [41].

Since the silica substrate cannot withstand temperatures higher than 1200 °C in the hot-wall configuration, only a narrow operating temperature window is allowed. Since the deposition rate is

apparently not thermally activated, the gas flow rate (or the residence time) appears as a key parameter for elaboration of long and thick tubes.

The gradual decomposition of DCMS above 700°C corresponds to the formation of various products in the gas phase. The apparition of methane and hydrogen chloride, both stable species, is progressive and tends to a plateau for the highest temperatures. The formation and consumption of the various chlorosilanes appearing successively (Figure 8) is apparently strongly related to the silicon incorporation in the coating.

A decomposition route of the DCMS during the APCVD process can be tentatively proposed by the analysis of the above results and the previous conclusions from the literature. Zhang and Hüttinger [21-38] proposed a mechanism for the deposition of SiC at near atmospheric pressure from the MTS/H_2 mixture, as did Cagliostro *et al*. for DCDMS [41]. As for MTS, the Si-C bond is probably readily dissociated into $CH_3^{\bullet}$ and $HSiCl_2^{\bullet}$ radicals in the hot zone [21, 42-44]. This assumption was confirmed by the *ab initio* calculations of Allendorf *et al*. [44]. The Si-H bond of DCMS or $HSiCl_2^{\bullet}$ is also probably easily broken to form eventually $SiCl_2$, likely a major silicon source for the coating [21, 42-44]. In parallel, $CH_3^{\bullet}$ readily recombines into CH_4, which is thermally stable and has a low surface reactivity. The chlorosilanes and $SiCl_4$ detected by FTIR result from the recombination of the $HSiCl_2^{\bullet}$ and $SiCl_2$ radicals, in the hot zone or during the cooling. The higher reactivity of $SiCl_2$ compared to CH_4 is responsible for the presence of excess silicon, especially at low temperatures and high α ratios. At high temperature (T > 1050 °C), the depletion of the most surface reactive silicon species in favor of $SiCl_4$, the HCl concentration increase, inhibiting Si-deposition [29, 41, 43], and finally the formation of more reactive unsatured hydrocarbons such as C_2H_2 (detected at 1200 °C and above), might be responsible for the increase of the carbon ratio in the coating. On the other hand, a higher H_2 concentration (higher α) promotes the reduction of $SiCl_2$ and therefore the deposition of free silicon, as well as the formation of CH_4, which limits the deposition of carbon.

6. Conclusions

Long and dense monolithic SiC tubes with thick walls were synthesized by CVD at atmospheric pressure inside a SiO_2 tube covered with pyrocarbon. An optimization of the process was carried out by analyzing the influence of different parameters such as the DCMS dilution in hydrogen, the total flow rate and the deposition temperature. The increase of deposition rate with the gas flow rate, and the low thermal activation of the deposition process indicate that the process is limited by mass transfer. Significant changes in the composition of the coating are observed when the deposition temperature and the H_2/DCMS ratio vary. This is related to the homogeneous reactions occurring in the reactor.

A FTIR spectroscopy analysis of the gas phase at the reactor outlet allowed its evolution to be followed versus temperature. The analysis of pure species such as DCMS, $HSiCl_3$ and $SiCl_4$ allowed the experimental assessment the values of molar absorptivities and the quantification of these products in the gas mixture. The successive production of SiH_2Cl_2, $SiHCl_3$ and $SiCl_4$ with an explicit lineage was highlighted, along with a continuous production of CH_4 and HCl. The increase of temperature induces a depletion of the reactive silicon species (e.g. $SiCl_2$) and could also promote the reactivity of the carbon precursors. On the other hand an important dilution in H_2 inhibits the carbon deposition and favors the reduction of chlorosilanes, hence resulting in a Si-rich deposit.

A thermodynamic study of the DCMS/H_2 system is currently being carried out in parallel to this experimental work.

The continuous synthesis of longer silicon carbide tubes by sliding of the heating coil along the substrate was successfully achieved, confirming the potential of the continuous deposition process for industrial purposes.

The mechanical testing of the samples by C-ring compression tests is in progress and should provide mechanical properties of these CVD-SiC tube structures.

Acknowledgements

The authors also thank E. Bruneton and P. David for fruitful discussion on the project, and both CEA and CNRS for their financial support.

References

[1] C. Lorrette, C. Sauder, L. Chaffron, "Progress in developing SiC/SiC composite materials for advanced nuclear reactors", ICCM 18, Jeju Island, Korea (2011) 1-4

[2] C. Ayranci, J. Carey, Compos. Struct. 85 (2008) 43–58

[3] R.H. Jones, L.L. Snead, A. Kohyama, P. Fenici, Fusion Eng. Des. 41 (1998) 15-24

[4] L. Brunel, N. Chauvin, T. Mizuno, M.A. Pauchon, J. Somers, The generation IV project GFR fuel and other core materials, GIF symposium – GEN IV international forum, 2009, Paris, France (2009), pp. 135–141

[5] R.H. Jones, L. Giancarli, A. Hasegawa, Y. Katoh, A. Kohyama, B. Riccardi *et al.*, J. Nucl. Mater. 307 (2002) 1057–1072

[6] Y. Katoh, A. Kohyama, T. Hinoki, L.L. Snead, Fusion Sci. Technol. 44 (2003) 155-162

[7] E.V. Dyomina, P. Fenici, V.P. Kolotov, M. Zucchetti, J. Nucl. Mater. 258-263 (1998) 1784-179

[8] A.R. Raffray, R. Jones, G. Aiello, M. Billone, L. Giancarli, H. Golfier *et al.*, Fusion Eng. Des.55 (2001) 55-95

[9] B. Riccardi, L. Giancarli, A. Hasegawa, Y. Katoh, A. Kohyama, R.H. Jones, L.L. Snead, J. Nucl. Mater. 329-333 (2004) 56-65

[10] H. Feinroth, B.R. Hao, "Multi-Layered Ceramic Tube for Fuel Containment Barrier And Other Applications In Nuclear And Fossil Power Plants", Patent WO2006/076039, (2006)

[11] C. Sauder, C. Lorrette, "Method for Producing a Composite Including a Ceramic Matrix", Patent WO2012/119805, (2012)

[12] G. Chollon, R. Naslain, C. Prentice, R. Shatwell, P. May, J. Eur. Ceram. Soc. 25 (2005) 1929-1942

[13] T.T. Cheng, I.P. Jones, R.A. Shatwell, P. Doorbar, Mater. Sci. Eng., A 260 (1999) 139-145

[14] O. Féron, G. Chollon, F. Dartigues, F. Langlais, R. Naslain, Diamond Relat. Mater. 11 (2002) 1234-1238

[15] S. Puntambekar, PhD thesis, University of Leicester (1995)

[16] P. Drieux, G. Chollon, A. Allemand, S. Jacques, Ceram. Trans. 240, Processing and Properties of Advanced Ceramics and Composites V, N.P. Bansal, J.P. Singh, S. Won Ko, R.H.R. Castro, G. Pickrell, N.J. Manjooran, M. Nair, and G. Singh, Editors (2013), *in press*

[17] M. J. Frisch, G.W. Trucks, H.B. Schlegel, G.E. Scuseria, M.A. Robb, J.R. Cheeseman, G. Scalmani, V. Barone, B. Mennucci, G.A. Petersson, H. Nakatsuji, M. Caricato, X. Li, H.P. Hratchian, A.F. Izmaylov, J. Bloino, G. Zheng, J.L. Sonnenberg, M. Hada, M. Ehara, K. Toyota, R. Fukuda, J. Hasegawa, M. Ishida, T. Nakajima, Y. Honda,O. Kitao,H. Nakai, T Vreven, J.A. Montgomery, Jr, J.E. Peralta, F. Ogliaro, M. Bearpark, J.J Heyd, E. Brothers,K.N. Kudin, V.N. Staroverov, R. Kobayashi, J. Normand,

K. Raghavachari,A. Rendell, J.C. Burant, S.S. Iyengar, J. Tomasi, M. Cossi, N. Rega, N.J. Millam, M. Klene, J.E. Knox, J.B. Cross, V. Bakken, C. Adamo,J. Jaramillo, R. Gomperts, R.E. Stratmann, O. Yazyev, A.J. Austin, R. Cammi, C. Pomelli, J.W. Ochterski, R.L. Martin, K. Morokuma, V.G. Zakrzewski, G.A. Voth,P. Salvador, J.J. Dannenberg, S. Dapprich, A.D. Daniels, Ö. Farkas, J.B. Foresman, J.V. Ortiz,J. Cioslowski, D.J. Fox, *Gaussian 09*, revision A.1, Gaussian Inc., Wallingford CT, (2009).

[18] C. Lee, W. Yang, R. G. Parr, Phys. Rev. B 37 (1988), 785.

[19] A. D. Becke, J. Chem. Phys. 98 (1993), 5648.

[20] A. Allouche, B. Pourcin, Spectrochim. Acta 49A (1993), 571.

[21] G. Chollon, F. Langlais, M. Placide, P. Weisbecker, Thin Solid Films 520 (2012) 6075-6087

[22] D.E. Cagliostro and S.R. Riccitiello, J. Am. Ceram. Soc. 73 (1990) 607-614

[23] W.G. Zhang, K.J. Hüttinger, Chem. Vap. Deposition 7 (2001) 173-181

[24] D.W. Feldman, J.H. Parker, W.J. Choyke, Physical Review B 173 (1968)

[25] S. Jonas, W. S. Ptak, W. Sadowski, E. Walasek, C. Paluszkiewicz, J. Electrochem. Soc. 142 (1995) 2357-2362

[26] J. N. Burgess, T. J. Lewis, Chem. Ind. (1974) 76-77

[27] V. Hopfe, H. Mosebach, M. Erhard, M. Meyer, J. Mol. Struct. 347 (1995) 331-342

[28] G. Socrates, Infrared Characteristic Group Frequencies, third revised edition, John Wiley & Sons Ltd, New York, 2004

[29] K. Brennfleck, S. Schneweis, R. Weiss, J. Phys. IV 9 (1999) 1041-1048

[30] J. Heinrich, S. Hemeltjen, G. Marx, Mikrochim. Acta 133 (2000) 209-214

[31] G.D. Papasouliotis, V. Sotirchos, J. Electrochem Soc. 141 (1994) 1599-1611

[32] Y. Ge and M.S. Gordon, J. Phys. Chem. A 111 (2007) 1462-1474

[33] T.M. Besmann, B.W. Sheldon, T.S. Moss, M.D. Kaster, J. Am. Ceram. Soc. 75-10 (1992) 2899-2903

[34] J.E. Marra, E.R. Kreidler, N.S. Jacobson, D.S. Fox, J Am Ceram Soc 71 (1988) 1067-1073

[35] G. Astarita, Ind. Eng. Chem. 58 (1966) 18-26

[36] F. Langlais, C. Prebende, B. Tarride, R. Naslain, J. Phys. Colloq. 50 (1989) 93-103

[37] H. Vincent, C. Vincent, L. Oddou, J. Bouix, T. S. Kannan, J. Mater. Chem. (1992) 567-574

[38] J.J. Brennan, Mater. Sci. Eng., A 126 (1990) 203-223

[39] D.E. Cagliostro and S.R. Riccitiello, J. Am. Ceram. Soc. 76 (1993) 49-53

[40] D.E. Cagliostro and S.R. Riccitiello, J. Am. Ceram. Soc. 77 (1994) 2721-2726

[41] G.D. Papasouliotis, S.V. Sotirchos, J. Mater. Res. 14 (1999), 3397-3409

[42] W.G. Zhang, K.J. Hüttinger, Chem. Vap. Deposition 7 (2001) 167-172

[43] F. Loumagne, F. Langlais, R. Naslain, J. Cryst. Growth 155 (1995) 205-213

[44] M.D. Allendorf, C.F. Melius, J. Phys. Chem. 97 (1993) 720-728

Table I. Deposition conditions for the synthesis of SiC tubes in static configuration

N°	Q_{tot} (sccm)	$\alpha = Q_{H2}/Q_{DCMS}$	T (°C)	Si $\%_{at.}$	Deposition rate (µm/h)
1	500	0	1100	45 to 60	N/A
2	500	1	1100	52	620
3	500	2	1100	55	910
4	500	4	1100	58	930
5	500	8	1100	65	650
6	500	12	1100	68	510
7	1000	4	1100	65	1170
8	250	4	1100	51	440
9	500	4	1125	58	990
10	500	4	1150	53	1080
11	500	4	1175	51	1110
12	500	4	1200	49	960

Table II. Frequencies (in this study) of the main IR features, assignment and literature values

Observed frequencies (cm^{-1})	Assignment	Chemical compound	Literature values
590	$\nu_a(SiCl_3)$	$SiHCl_3$	585, 592 [26]
620	$\nu_a(SiCl_4)$	$SiCl_4$	619 [26], 620 [25]
756	$\nu(SiC)$	DCMS	752, 762 [26]
807	$\delta(HSiCl)$	$SiHCl_3$	805 [28]
852	$\delta(HCSi)$ + $\delta(HSiCl)$	DCMS	[25] [29]
889			
949	$\delta(SiH_2)$	SiH_2Cl_2	960 [26]
1268	$\delta_s(CH_3)$	DCMS	1270 [26], 1272 [25]
1307	$\delta_a(CH_4)$	CH_4	1305 [25], 1306 [27], 1310 [26]
2217	$\nu(SiH)$	DCMS	2220 [28]
2260	$\nu(SiH)$	$SiHCl_3$	2260 [25], 2270 [26]
2984	$\nu_a(CH_3)$	DCMS	-
3017	$\nu_a(CH_4)$	CH_4	3018 [26]
2700-3100	$\nu(HCl)$ vibro-rotation	HCl	2700-3095 [26] [30]

ν : stretching; δ : bending; a : antisymmetric; s : symmetric

Figure 1. APCVD reactor for SiC deposition

Figure 2. (a) Cross section of the SiO_2/PyC/SiC interfacial region. (b) Extracted SiC tube (T = 1200 °C, Q_{tot} = 500 sccm, α = 2, v = 0.25 cm/min)

Figure 3. Influence of α (a), T (b) and Q_{tot} (c) on the Raman features

Figure 4. Temperature (T), thickness (e) and composition (Si atomic concentration) longitudinal profiles of a coating synthesized in static configuration (α = 4, T_{max} = 1100 °C, Q_{tot} = 500 sccm)

Figure 5. Radial EPMA (a) and Raman (b) profile of a thick SiC tube (α = 2, Q = 1000 sccm, T = 1200 °C)

Figure 6. Experimental IR spectra of pure species (CH4, HCl, $SiCl_4$, $HSiCl_3$, CH_3HSiCl_2)

Figure 7. IR spectra of the gas phase (Q_{tot} = 500 sccm, α = 4, P_{atm}) as a function of T in 3200 – 2800 cm^{-1} (a), 2300 – 2150 cm^{-1} (b), 1360 – 1200 cm^{-1} (c) and 1000 – 600 cm^{-1} (d) frequency domains

Figure 8. Concentration of the various species in the gas phase (Q_{tot} = 500 sccm, α = 4, P_{atm}) as a function of T

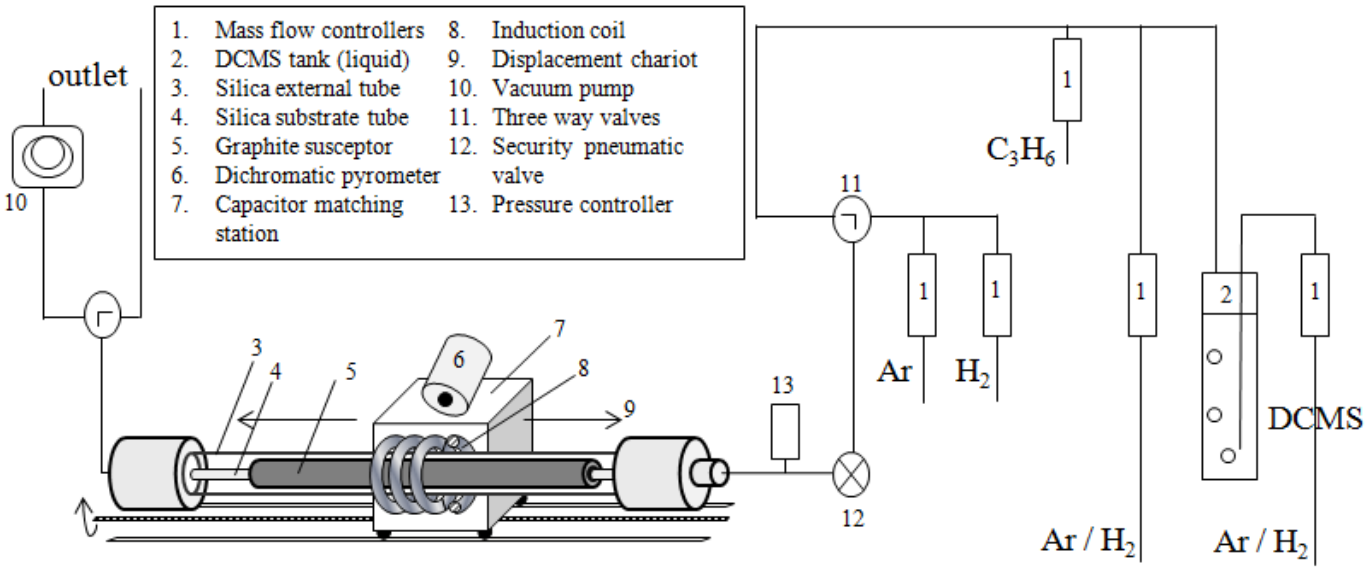

Figure 1

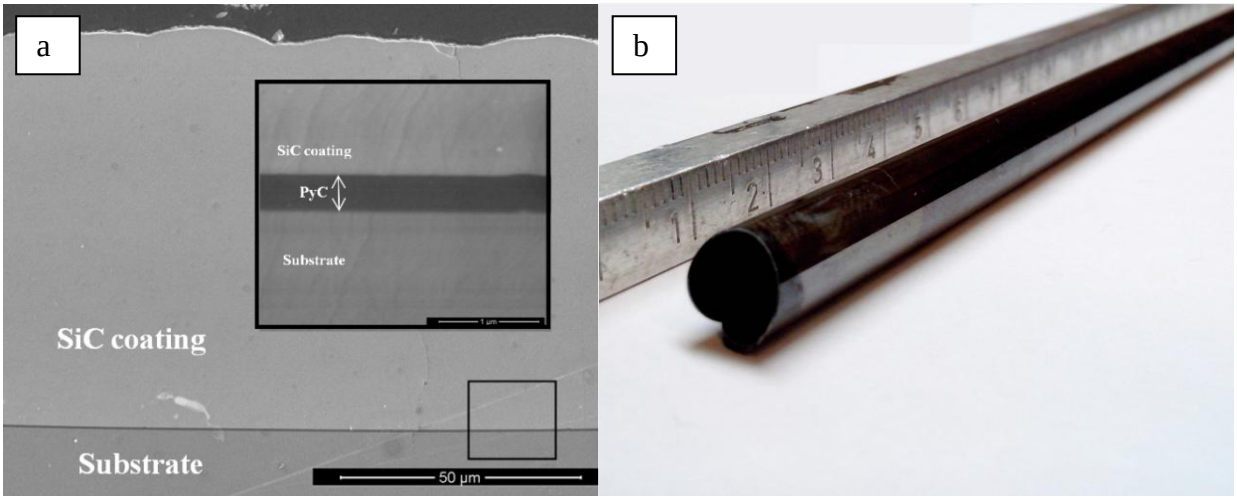

Figure 2

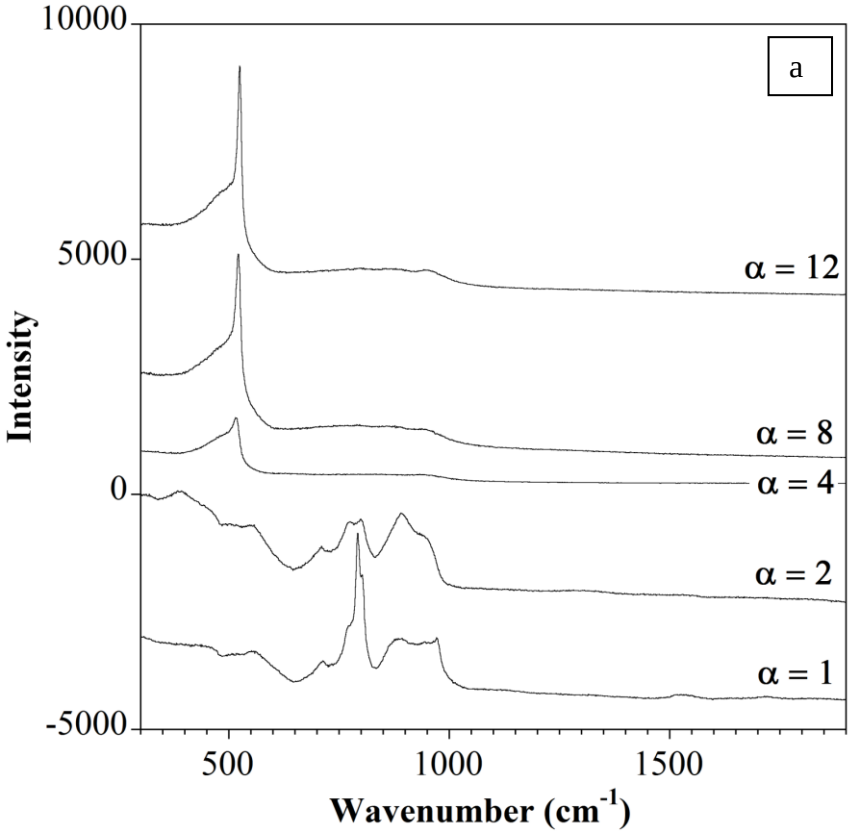
a
10000
5000
0
-5000
Intensity
α = 12
α = 8
α = 4
α = 2
α = 1
500
1000
1500
Wavenumber (cm-1)

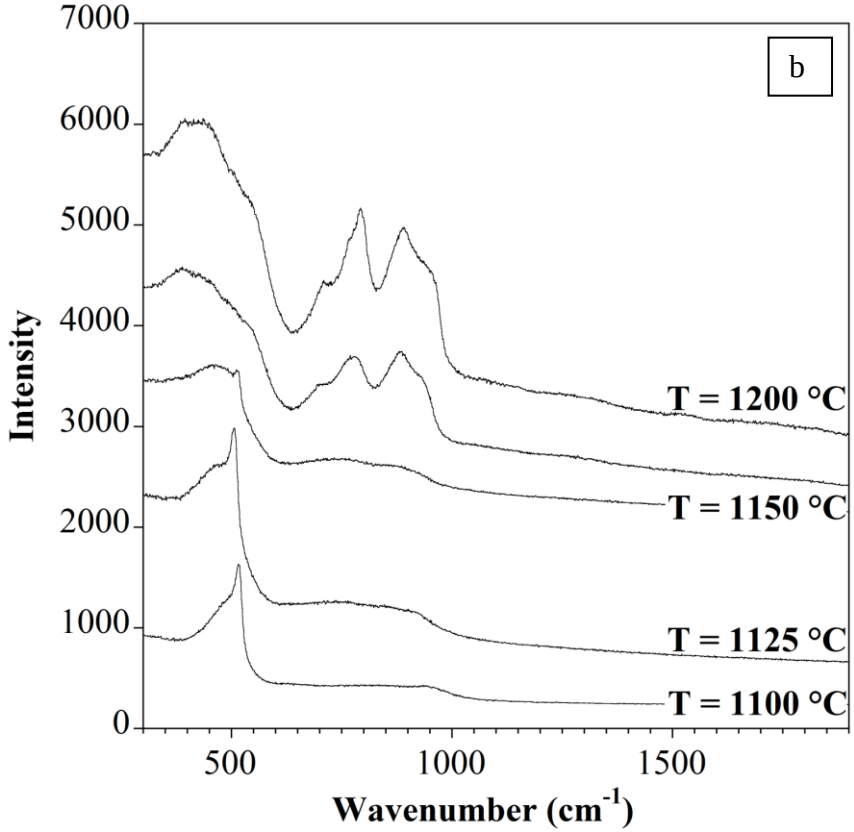
b
7000
6000
5000
4000
3000
2000
1000
0
Intensity
T = 1200 °C
T = 1150 °C
T = 1125 °C
T = 1100 °C
500
1000
1500
Wavenumber (cm-1)

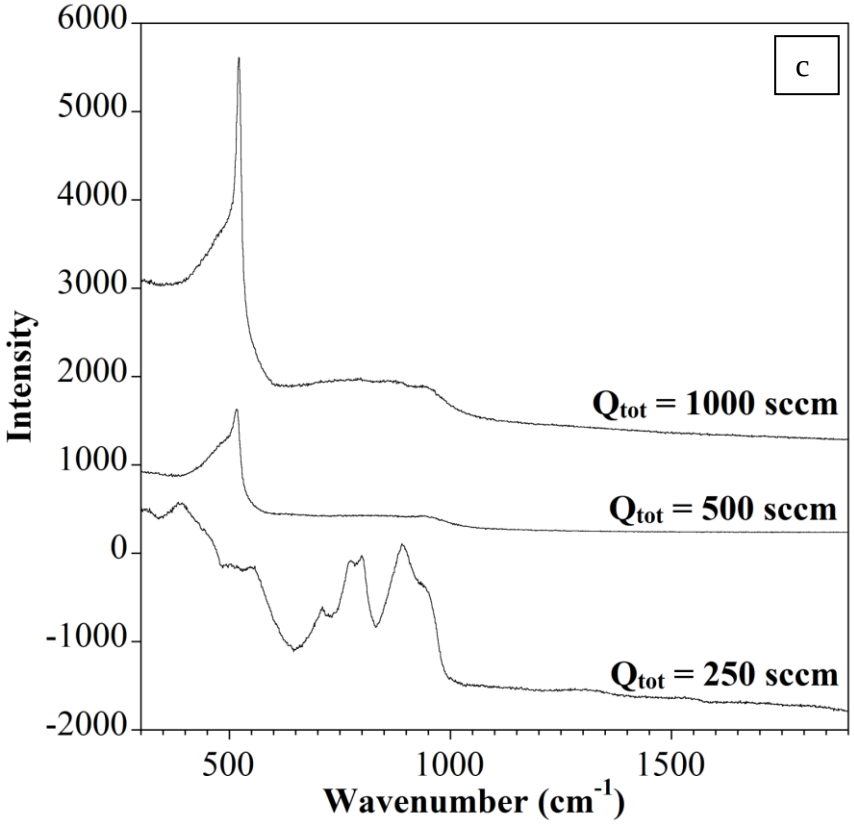

Figure 3

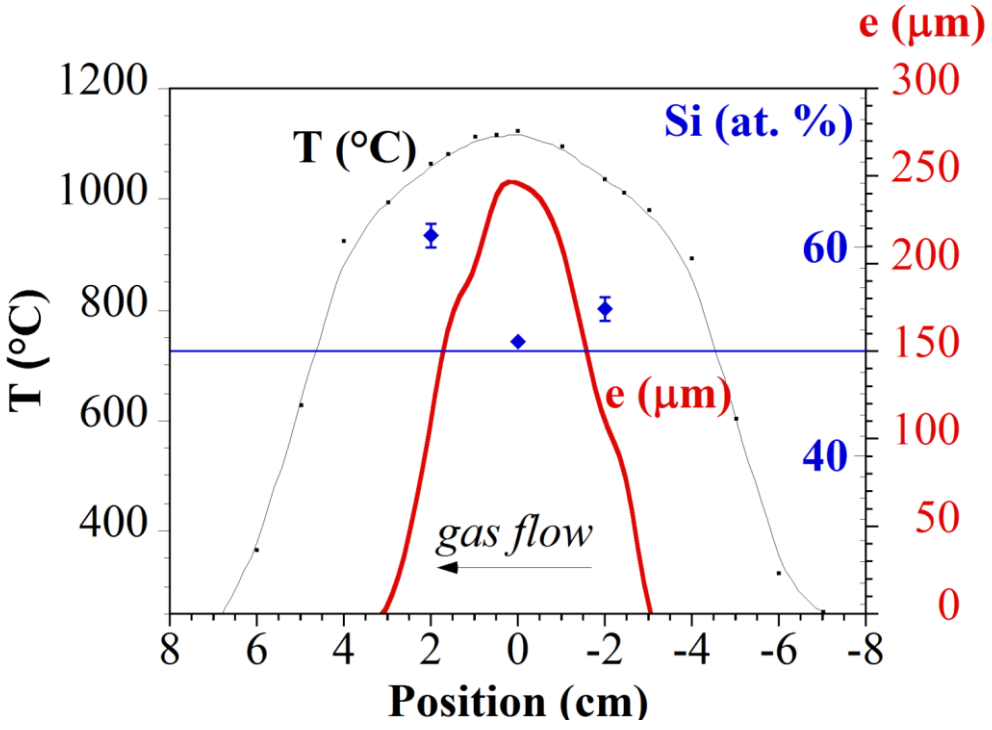

Figure 4

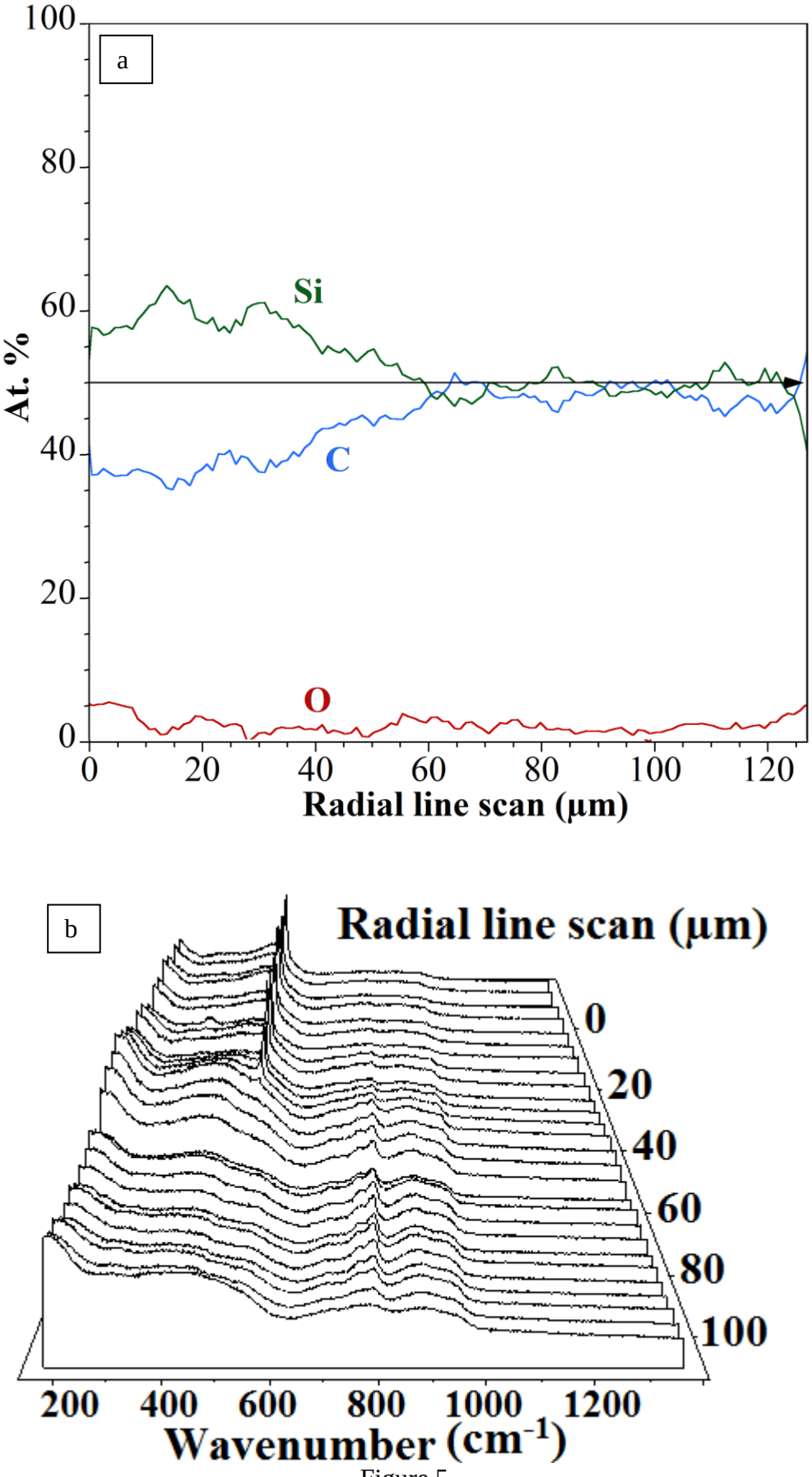
a
100
80
60
40
20
0
At. %
Si
C
O
0
20
40
60
80
100
120
Radial line scan (μm)
b
Radial line scan (μm)
0
20
40
60
80
100
200
400
600
800
1000
1200
Wavenumber (cm-1)

Figure 5

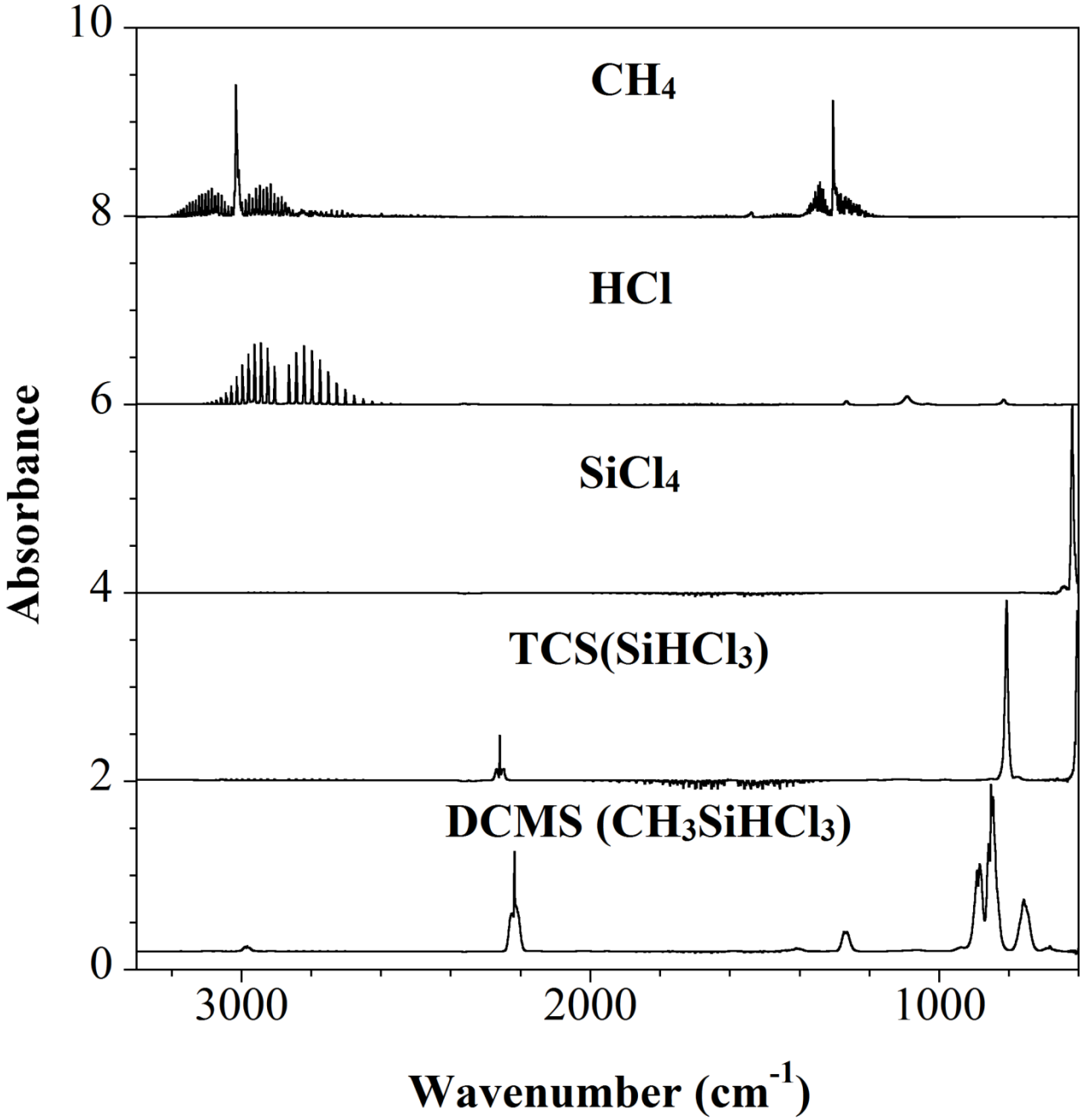
10
8
6
4
2
0
Absorbance
CH4
HCl
SiCl4
TCS(SiHCl3)
DCMS (CH3SiHCl3)
3000
2000
1000
Wavenumber (cm-1)

Figure 6

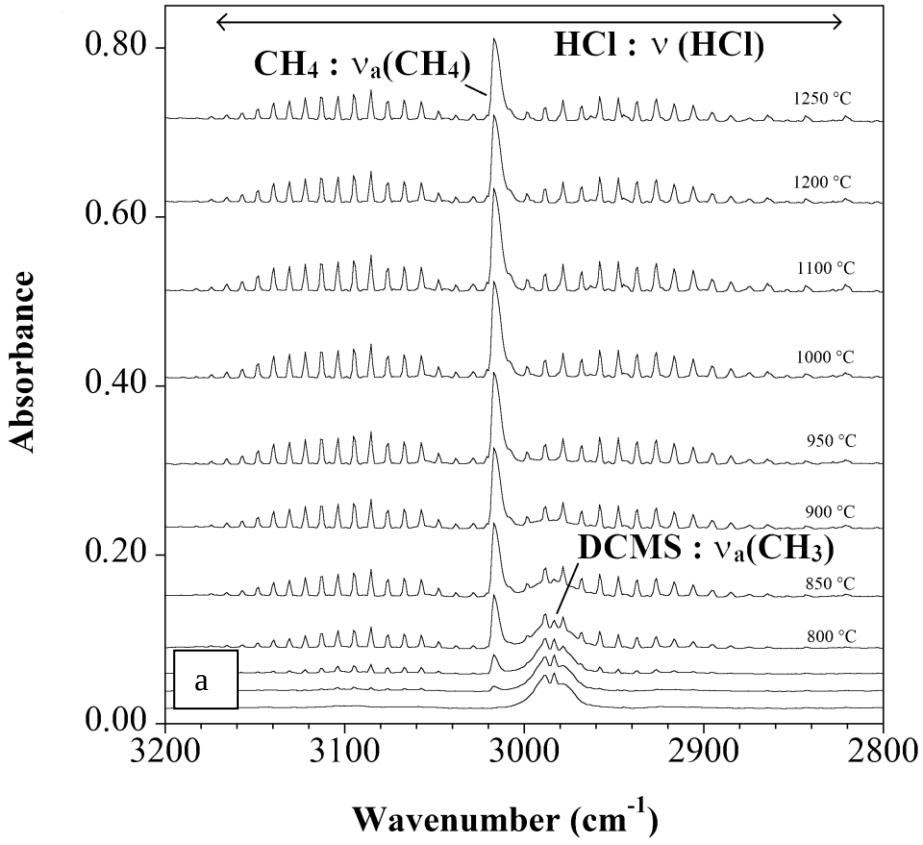
HCl : ν (HCl)
CH4 : νa(CH4)
1250 °C
1200 °C
1100 °C
1000 °C
950 °C
900 °C
DCMS : νa(CH3)
850 °C
800 °C
a
Absorbance
0.80
0.60
0.40
0.20
0.00
3200
3100
3000
2900
2800
Wavenumber (cm-1)

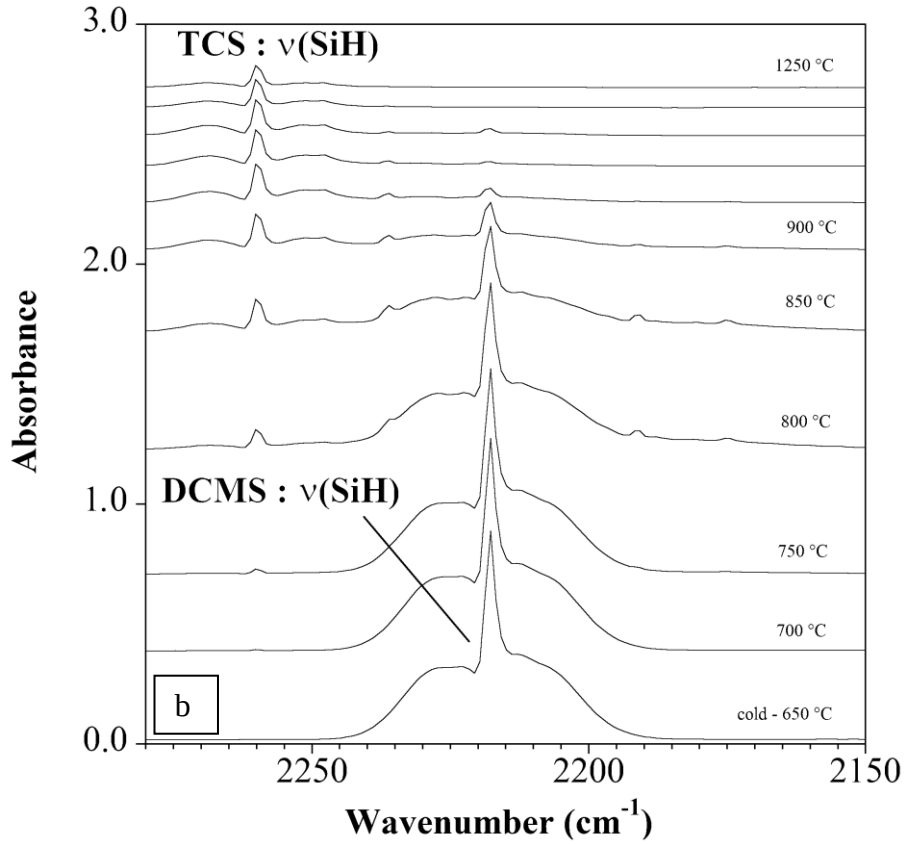
TCS : ν(SiH)
1250 °C
900 °C
850 °C
800 °C
DCMS : ν(SiH)
750 °C
700 °C
cold - 650 °C
b
Absorbance
3.0
2.0
1.0
0.0
2250
2200
2150
Wavenumber (cm-1)

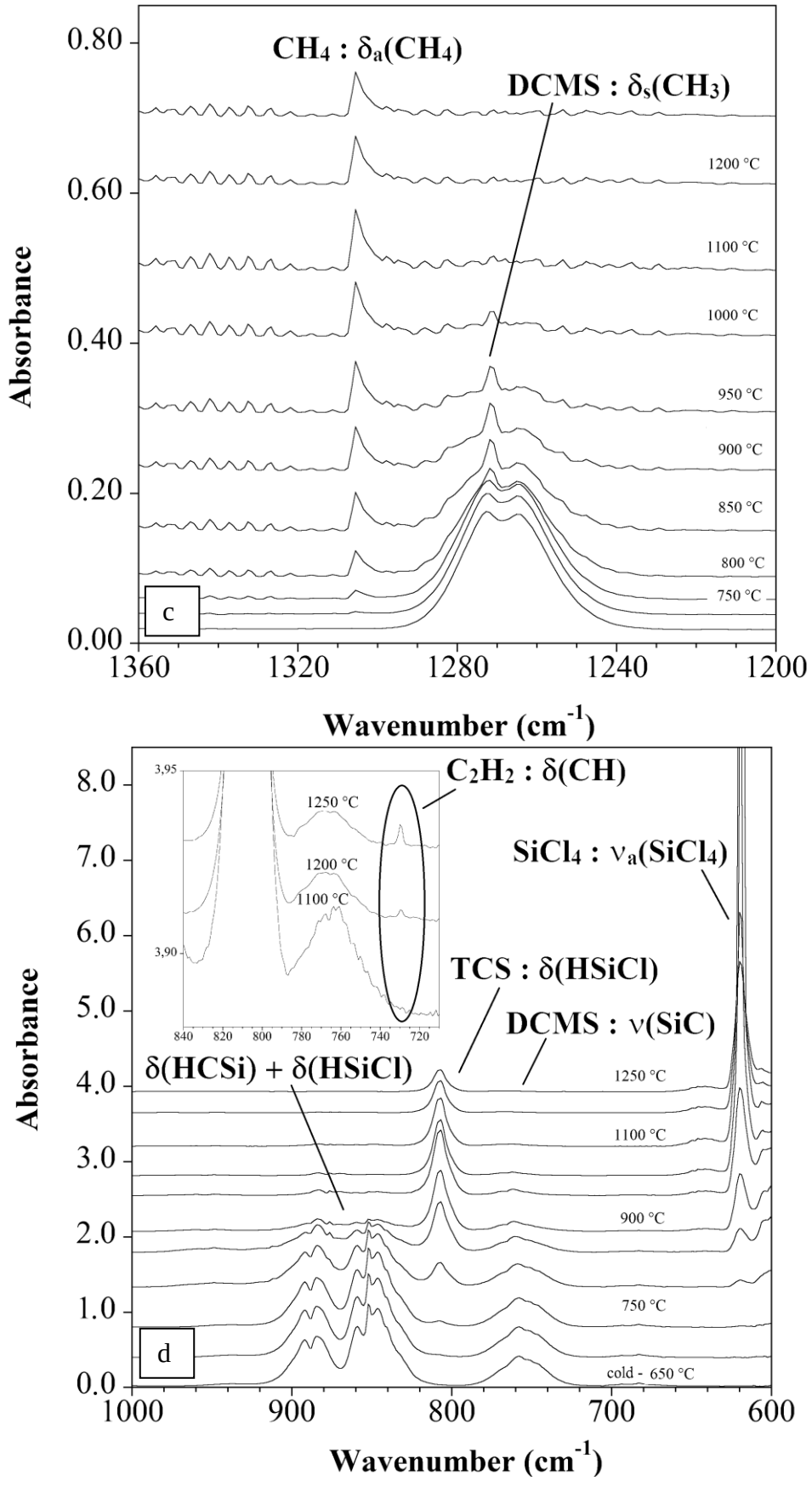
CH4 : δa(CH4)
DCMS : δs(CH3)
1200 °C
1100 °C
1000 °C
950 °C
900 °C
850 °C
800 °C
750 °C
c
Absorbance
Wavenumber (cm-1)
C2H2 : δ(CH)
SiCl4 : νa(SiCl4)
TCS : δ(HSiCl)
DCMS : ν(SiC)
δ(HCSi) + δ(HSiCl)
1250 °C
1100 °C
900 °C
750 °C
cold - 650 °C
d
Absorbance
Wavenumber (cm-1)

Figure 7

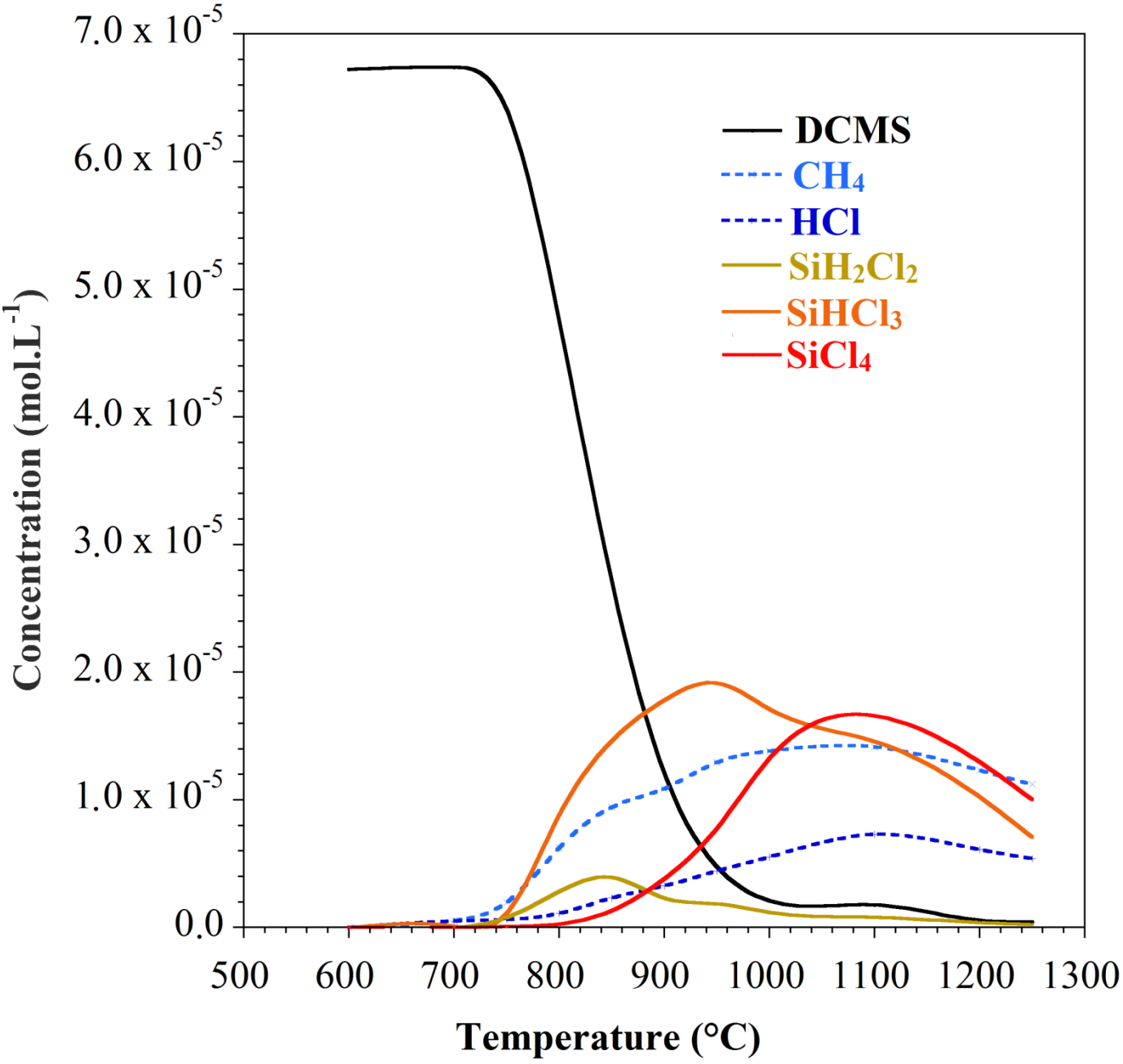
7.0 x 10-5
6.0 x 10-5
5.0 x 10-5
4.0 x 10-5
3.0 x 10-5
2.0 x 10-5
1.0 x 10-5
0.0
Concentration (mol.L-1)
500
600
700
800
900
1000
1100
1200
1300
Temperature (°C)
DCMS
CH4
HCl
SiH2Cl2
SiHCl3
SiCl4

Figure 8